
**AFRL-AFOSR-JP-TR-2023-0092**

# Developing graphene Josephson microwave single-photon detectors for quantum information science

**Englund, Dirk**
**MASSACHUSETTS INST OF TECH LEXINGTON**
**244 WOOD ST**
**LEXINGTON, MA,**
**US**

**08/06/2023**
**Final Technical Report**



Air Force Research Laboratory
Air Force Office of Scientific Research
Asian Office of Aerospace Research and Development
Unit 45002, APO AP 96338-5002

# REPORT DOCUMENTATION PAGE

**PLEASE DO NOT RETURN YOUR FORM TO THE ABOVE ORGANIZATION.**

| 1. REPORT DATE | 2. REPORT TYPE | 3. DATES COVERED | |
|---|---|---|---|
| 20230806 | Final | START DATE<br>20200930 | END DATE<br>20230329 |

**4. TITLE AND SUBTITLE**
Developing graphene Josephson microwave single-photon detectors for quantum information science

| 5a. CONTRACT NUMBER | 5b. GRANT NUMBER | 5c. PROGRAM ELEMENT NUMBER |
|---|---|---|
| | FA2386-20-1-4070 | |
| **5d. PROJECT NUMBER** | **5e. TASK NUMBER** | **5f. WORK UNIT NUMBER** |
| | | |

**6. AUTHOR(S)**
Dirk Englund

**7. PERFORMING ORGANIZATION NAME(S) AND ADDRESS(ES)**
MASSACHUSETTS INST OF TECH LEXINGTON
244 WOOD ST
LEXINGTON, MA
US

**8. PERFORMING ORGANIZATION REPORT NUMBER**

| 9. SPONSORING/MONITORING AGENCY NAME(S) AND ADDRESS(ES) | 10. SPONSOR/MONITOR'S ACRONYM(S) | 11. SPONSOR/MONITOR'S REPORT NUMBER(S) |
|---|---|---|
| AOARD<br>UNIT 45002<br>APO AP 96338-5002 | AFRL/AFOSR IOA | AFRL-AFOSR-JP-TR-2023-0092 |

**12. DISTRIBUTION/AVAILABILITY STATEMENT**
A Distribution Unlimited: PB Public Release

**13. SUPPLEMENTARY NOTES**

**14. ABSTRACT**
During this program we (1) Developed milliKelvin optical scanning capabilities, (2) Demonstrated single-infrared photon calorimetry, a departure from conventional single-photon detectors (SPDs) where energy resolution is no longer limited by an energy gap, (3) Detected single-infrared (1550 nm) photons through graphene calorimetry with quantum efficiencies of ~90%, (4) Studied the spatial heat propagation in graphene, (5) Augmented the operation temperature of JJ-based SPD up to 1.2 K, a new record for this SPD platform, (6) Studied theoretically the dissipative heat diffusion of the heat from a single photon so that we can predict and optimize the SPD performance.

**15. SUBJECT TERMS**

| 16. SECURITY CLASSIFICATION OF: | | | 17. LIMITATION OF ABSTRACT | 18. NUMBER OF PAGES |
|---|---|---|---|---|
| a. REPORT<br>U | b. ABSTRACT<br>U | c. THIS PAGE<br>U | SAR | 7 |

| 19a. NAME OF RESPONSIBLE PERSON | 19b. PHONE NUMBER *(Include area code)* |
|---|---|
| MICHAEL RICHARDS | 3152277000 |

**Standard Form 298** (Rev.5/2020)
Prescribed by ANSI Std. Z39.18

# AFOSR Final Report for June 2023

| | |
|---|---|
| **Project Title** | Developing graphene Josephson microwave single-photon detectors for quantum information science |
| **Agency** | Asian Office of Aerospace Research and Development |
| **Principal Investigators** | Dirk Robert Englund (englund@mit.edu, 617-324-7014)<br>Gil-Ho Lee (lghman@postech.ac.kr, +82 054-279-6704) |
| **Collaborator** | Kin Chung Fong (kc.fong@rtx.com, 617-873-3316) |
| **Program Manager** | Michael J. Richards, Lt. Col., USAF |
| **Performance Period** | 9/2020 - 3/2023 |

1. **Achievements of this project:**

   During this program we:

   1. Developed milliKelvin optical scanning capabilities
   2. Demonstrated single-infrared photon calorimetry, a departure from conventional single-photon detectors (SPDs) where energy resolution is no longer limited by an energy gap.
   3. Detected single-infrared (1550 nm) photons through graphene calorimetry with quantum efficiencies of ~90%
   4. Studied the spatial heat propagation in graphene.
   5. Augmented the operation temperature of JJ-based SPD up to 1.2 K, a new record for this SPD platform.
   6. Studied theoretically the dissipative heat diffusion of the heat from a single photon so that we can predict and optimize the SPD performance.

These findings are currently being summarized in at least two manuscripts that are in preparation and which we detail below.

2. **Achievements**

A. milliKelvin Optical Scanner

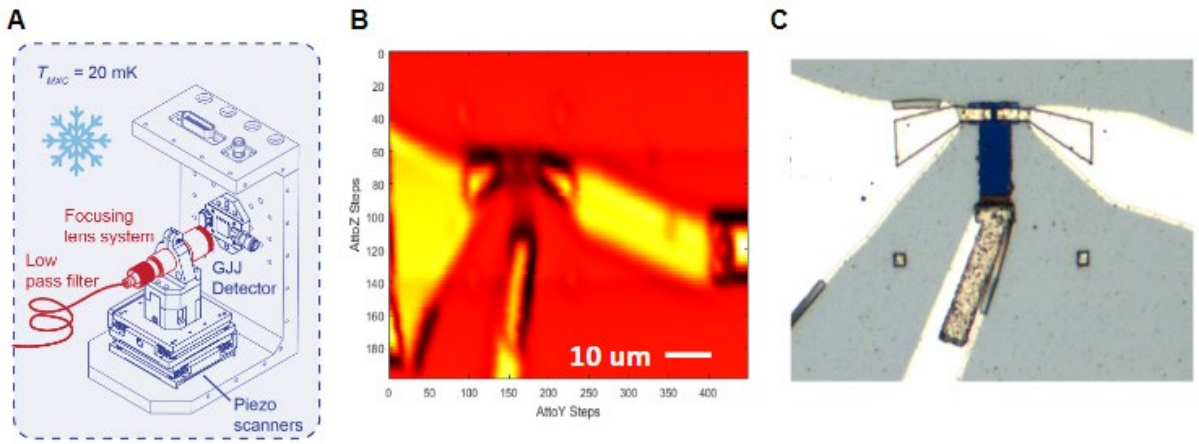


**Figure 1: MilliKelvin scanning optical reflectometry. (A)** Schematic of the milliKelvin scanner in the mixing chamber of the dilution refrigerator. 1550 nm infrared light is coupled to our graphene Josephson junction (gJJ) single-photon detector (SPD) via a low-passed optical fiber and focusing lens assembly. The fiber-lens assembly is mounted on a three-axis piezoelectric scanner. These scanners, when actuated, allow full control over the position of the laser spot on the gJJ detector, which is anchored to the mixing chamber. **(B)** 2D optical reflectometry scan of a gJJ SPD at T ~ 100 mK. **(C)** Optical micrograph of the same gJJ SPD shown in **(B)** taken at room temperature.

We have developed a milliKelvin optical scanning setup whereby a focusing lens assembly is attached to a three-axis piezoelectric scanner (Figure 1A). The scanner allows for both focusing and positioning of the lens assembly to within several hundred nanometers of accuracy. The lens is connected to a room-temperature optical setup through an optical fiber and is optimized to admit wavelengths of 1550 nm. In Figure 1B, we scan a graphene device (Figure 1C) using standard optical reflectometry techniques, while the fridge is at milliKelvin temperatures. This allows us to image the device, providing vital information on the location and focusing of our beam spot.

## B. Calorimetric SPD based on Graphene-Josephson Junction

In this section, we demonstrate the ability to detect the heat of a single infrared photon using an SNS graphene Josephson junction (gJJ). The basic scheme is illustrated in Figure 2A. Using the milliKelvin optical scanner described in the previous section we focus the lens over a long graphene ‘target’. Photons are emitted from the lens and absorbed by the graphene, causing a rise in electron temperature. These hot electrons diffuse towards the Josephson junction, which is biased just below the critical current. The incoming hot electrons heat the junction causing the device to transition from superconducting to normal, thus heralding the detection of a photon.

In Figure 2B we show one such calorimetric gJJ single-photon detector (SPD). Contact to graphene is made using molybdenum-rhenium, a type-II superconductor known for making high transparency contacts to graphene. The junction is 600 nm long and 1.7 um wide. The critical current can be electrostatically tuned using a graphite backgate, which also serves to screen the graphene from charge inhomogeneity. Attached to the junction is a 4 um by 25 um graphene extension, which serves as the ‘target’ for the infrared photons.

The single-photon detection scheme is as follows: the device is well described by the RCSJ model, whereby an imaginary phase particle resides inside the well of a tilted washboard potential (Inset Figure 2C). This potential is determined by the Josephson energy of the device. To aid in the detection,

the barrier can be reduced by applying a bias. If an incoming photon is absorbed by the graphene, the temperature of the device is elevated, reducing the barrier of the potential causing the phase particle to “run" down the well -- switching the device to normal. The normal state is then detected through the finite voltage of the normal state. Therefore, we sweep the current bias through the device and record the bias at which the junction switches. In Figure 3C, we report the switching rate of the junction as a function of current bias. We find that, when the laser is off, we retrieve the standard switching rate due to macroscopic quantum tunneling. However, when the laser is turned on, premature switching occurs at lower biases.

To investigate the nature of this premature switching we set the device to a fixed current bias (at ~80% of the critical current). The measurement scheme is such that we record when the device has switched from superconducting to normal. When this occurs the bias will drop to 0 allowing the device to switch back into the superconducting state, allowing us to measure the next switching event. We record the number of these events in a time window as a function of laser power, which allows us to extract the switching rate (Figure 2D). Importantly, we find that when time-binning our switching events the distributions as a function of laser power adhere to Poissonian statistics (inset Figure 2D). This indicates that our detector is photon shot-noise limited. Furthermore, by plotting the switching rate as a function of laser power we see a linear trend, indicating that our switching events are due to the detection of a single photon.

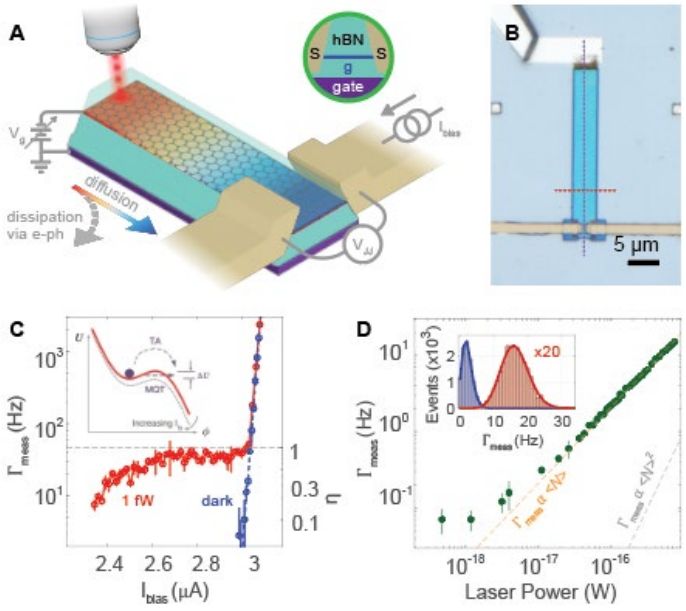


**Figure 2: Graphene-based calorimetric SPD. (A)** Illustration of the calorimetric SPD. The detector consists of a large graphene target and superconducting electrodes contacting one end of the target that form a gJJ. Single photons from an attenuated laser source are directed and focused onto the target, which get absorbed by the graphene and heats up the electrons. This heat diffuses out to the gJJ, lowering the critical current of the junction below an applied bias current, $I_{bias}$, and switches the junction to the normal state. This single-photon induced switching is detectable as a non-zero voltage across the junction, $V_{JJ}$. Inset shows the side profile of the gJJ. **(B)** Optical micrograph of a gJJ SPD. The dotted lines show the line cuts of the scanning data presented in Figure 3. JJ superconducting electrodes are

false-colored in yellow. **(C)** Junction switching rate vs. bias current applied to the junction when the graphene target is illuminated by single infrared photons (red) and when the illumination is turned off (blue). Inset: Current-biased JJ can be described as a macroscopic quantum phase particle subject to a tilted-washboard potential in the RCSJ model. **(D)** Junction switching rate vs. laser power incident on the graphene. The switching rate grows linearly vs. laser power (orange line) with an offset due to detector dark counts. Inset shows the distribution of junction rates from one-second photon counting experiments with a laser power of 60 aW (blue) and 500 aW (red). Poissonian fits (solid lines) to the distributions fit well, indicating that the switching events are indeed uncorrelated, single-photon switching events. Error bars span two standard deviations of error.

Next, we place the center of our beam spot 6 um away from the edge of the superconducting contact and demonstrate the geometric dependence of our laser spot by scanning the laser across the width of our graphene target. We first perform the reflectometry measurement to ensure that we are traversing the graphene 'target' (Figure 3A). The relative reflectance values of the graphene and substrate are consistent with values derived from thin-film interference calculations, and from a simple geometric convolution of the laser spot with the graphene device (solid line Figure 3A). Next, the laser power is fixed at 1 fW and we measure the switching rate of the device as we scan across the graphene (Figure 3B). Once again, we find that the switching rate is simply proportional to the geometric convolution between the beam spot and the graphene target: the switching rate is maximal when the beam spot is fully hitting the graphene, and drops off when the beam spot traverses off the graphene and onto the substrate. Finally, we demonstrate that the dominant source of change in the switching rate is geometric by taking the number of photons expected from our normalized convolution and retrieving the quantum efficiency as a function of position (Figure 3C). We again see that the quantum efficiency is flat when the beam is over the device and only increases when the beam is near the edge attributed to dark counts.

We now turn to scanning the laser across the vertical extent of the device. Once again, the reflectometry is used to map the device (Figure 3D). Next we measure the switching rate as a function of position away from the junction (Figure 3E). Again, we find that geometric effects dominate the switching rate. Remarkably, after the beam is fully contained within the graphene target, we observe a plateau in the switching rate. This indicates that the length of our device is less than the thermal length of the graphene. Notably, as the beam starts to convolve with the leads, we observe a sharp decrease in the switching rate. This is an important distinction with previous iterations of graphene photodetectors, which exploit a plasmon mode along a graphene-NbN interface to facilitate pair breaking in the junction. The observation of the downturn in switching rate shows that a plasmon mode is likely non-existent at the graphene-MoRe interface and plasmon-mediated absorption is not playing a role in our SPD.

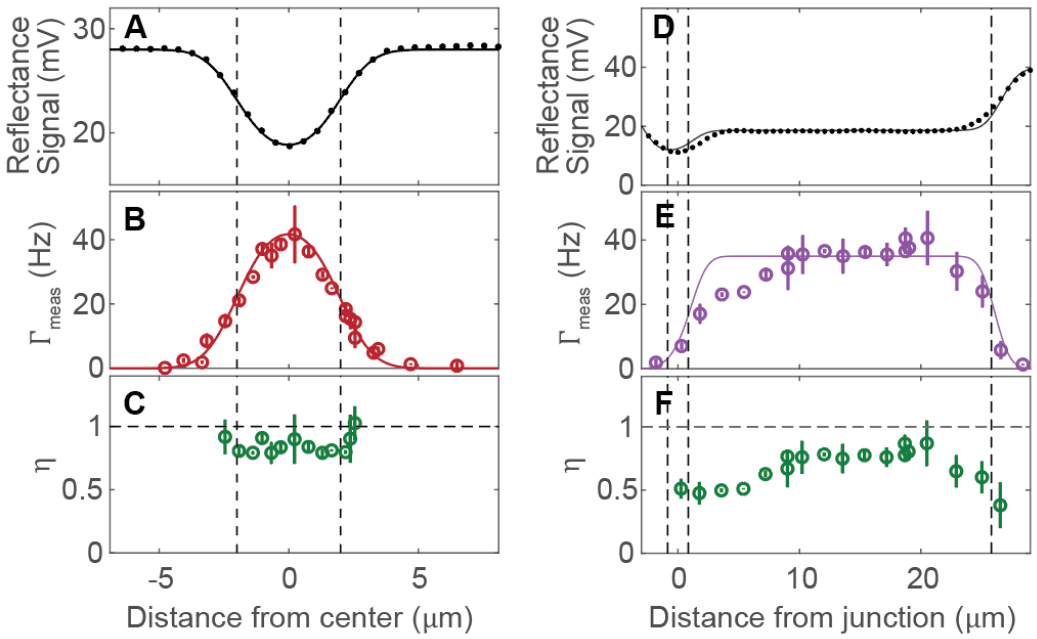


**Figure 3: Switching of the graphene Josephson junction** across **(A-C)** the width and **(D-F)** the length of the graphene target. Panels **(A)** and **(D)** show reflectometry data, panels **(B)** and **(E)** show junction switching rates, and panels **(C)** and **(F)** along each of the respective line cuts. The solid lines are fits of the reflectometry and single-photon counting data to reflectance and photon absorption values calculated from geometric convolution and thin-film interference. Error bars span two standard deviations of error.

We now turn to studying the effects of varying electron density on the single-photon detection. Figure 4A shows the switching rate and quantum efficiency as a function of bias as the backgate is tuned and with 1 fW of laser power incident on the graphene. We see that as the device is tuned away from the Dirac peak (at -0.15 V), the switching current increases, as expected for a typical graphene Josephson junction. Further, premature switching associated with absorption of a single infrared photon emerges. However, near $V_{bg}$ = 3.5 V, we find that the critical current saturates. Upon further gating, the premature switching vanishes entirely. This is fully seen in Figure 4B where we show the quantum efficiency as a function of normalized bias and backgate voltage. We suspect that this may be due to the increase in heat capacity as density is increased, however the gate tunability of the photon detection is further evidence that we are measuring a rise in the electronic temperature in graphene due to a single photon.

We can further characterize our device by comparing the quantum efficiency as a function of dark count rate (Figure 4C). We measure the switching rate with the laser off and extrapolate the dark count rate. We find that, near optimal gating, we maintain a quantum efficiency exceeding 80% with a dark count rate of one per several hours.

We then test the limits of the detector at elevated temperature. In Figure 5, we reproduce the linear dependence of switching rate on laser power from Figure 2D with a bath temperature of 1.2 K. This is an important milestone as it means our device can operate in a more conventional cryocooler setup, avoiding the need for milliKelvin temperatures in a bulky dilution refrigerator. It further sets the baseline record for temperature performance in this new paradigm of SPD.

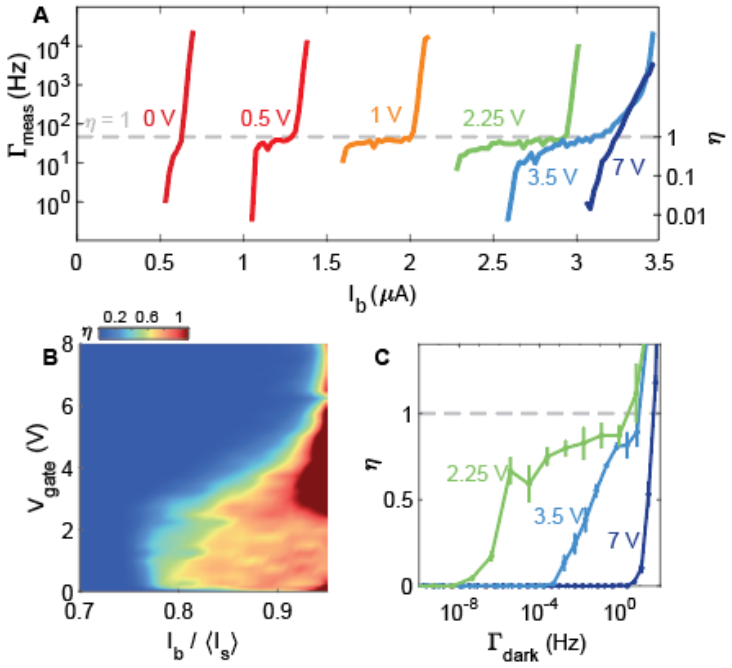


**Figure 4: Gate dependence and detector efficiency. (A)** Junction switching rate vs. bias current. The gray dashed line demarcates η = 1. **(B)** Color plots of η vs. $V_{gate}$ and normalized current bias, $I_b/\langle I_s \rangle$. **(C)** η vs. detector dark count at select gate voltages. Error bars span two standard deviations of error.

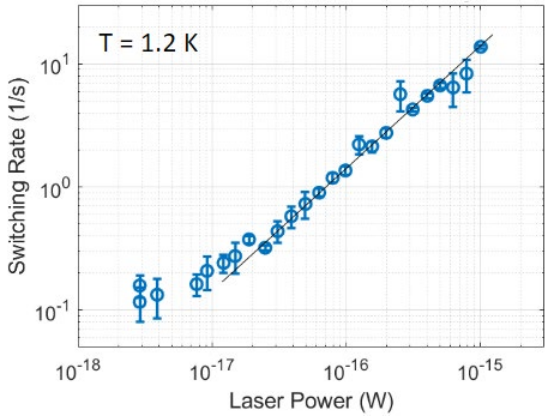


**Figure 5: Single-photon detection at 1.2 K.** Junction switching rate vs. laser power. The black solid line is a linear power law fit. The data fits well to the linear power law fit, indicating that single-photon detection is still possible at 1.2 K.

C. Calculations describing the thermal propagation in graphene due to a single photon

We solve the dissipation-diffusion equation to study the thermal propagation of a single infrared photon absorbed by a graphene target:

$$c_e \frac{\partial \Theta}{\partial t} = -\nabla(\kappa \nabla \Theta) - \Sigma(\Theta^{\delta} - \Theta_b^{\delta})$$

Where $C_e$ is the electronic heat capacity, $\Theta$ is the temperature, $\kappa$ is the thermal conductivity, $\Sigma$ is the electron-phonon coupling parameter, and $\delta$ is determined by the disorder in graphene. Figure 6 shows the temperature rise as a function of time at one end of the graphene when the graphene absorbs a photon. We cover the dirty (dissipation dominated) and clean (diffusion dominated) limits for different positions along the target and different target sizes. Here,

$$\tau_{th} = \frac{\gamma}{\delta \Sigma \theta_0^{\delta-2}}$$

is the thermal time constant, with γ the Sommerfeld constant and $l_{th}$ is the thermal length scale. We find substantial temperature rises at the graphene detector which can explain the high quantum efficiency of our calorimetric graphene SPD.

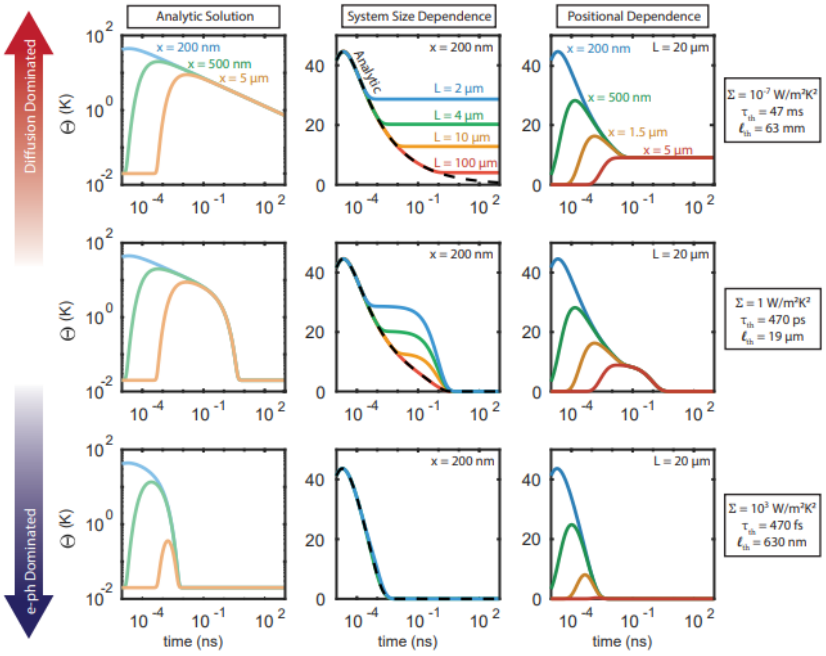


**Figure 6: Calculations of the electronic temperature rise in graphene due to an incident photon.** The temperature rise as a function of time is plotted for the analytic solution of the dissipation diffusion equation above, as well as for the diffusion dominated and dissipation dominated regimes. We study different system sizes, as well as the effect of moving the beam spot to a different position on the device.